IEEE Access
Multidisciplinary | Rapid Review | Open Access Journal

Received 3 January 2024, accepted 1 February 2024, date of publication 5 February 2024, date of current version 13 February 2024.

Digital Object Identifier 10.1109/ACCESS.2024.3362245

RESEARCH ARTICLE

Massive MIMO With Circular Antenna Array: Design, Implementation, and Validation

SPANDAN BISOYI[1], PASUPULETI MURALIMOHAN[1], HARISH KUMAR DUREPPAGARI[2], PAVAN REDDY MANNE[2], SAIDHIRAJ AMURU[1], AND KIRAN KUCHI[1], (Senior Member, IEEE)

[1]Department of Electrical Engineering, Indian Institute of Technology Hyderabad, Hyderabad 502284, India
[2]Wisig Networks Pvt. Ltd., Hyderabad 502284, India

Corresponding author: Spandan Bisoyi (ee17resch11002@iith.ac.in)

This work was supported in part by the Department of Electronics and Information Technology, Government of India, with Project Name "Converged Cloud Communication Technologies (CCRAN)" through Convergence, Communications & Broadband Technologies (CC&BT) under Grant R-23011/03/2014-R&D; and in part by the Department of Telecommunication Networks & Technologies Cell (DoT-NT-Cell), Government of India, with Project Name "Indigenous 5G Test Bed (Building an End to End 5G TestBed)" under Grant DoT-NT-Cell/EE/F072/2017-18/G129.

ABSTRACT Massive MIMO is a key technology for the current and next-generation cellular standards to achieve multi-fold improvements in the spectral efficiency of the network. Various demonstrations of this Massive MIMO technology in the existing literature transmit data to a maximum of 15 users simultaneously in the downlink while using 64 to 100 antenna ports at the base station. In this paper, we present in detail the design and implementation of our Large-scale Massive MIMO testbed, where we demonstrate a further maximization of the user pairing to realize the high network capacities achievable with massive MIMO technology. This is the first testbed implementation that demonstrates as high as 24 user pairing in downlink by utilizing 192 antenna elements (48 antenna ports) at the base station. This high user pairing capability helps the network operators to support as many users in a limited amount of spectrum and achieve multifold improvement in the network capacity. Further, this is a first step in the direction of understanding the real-world limitations of Massive MIMO systems in a variety of deployment scenarios and under constraints such as antenna array sizes, antenna array types such as circular versus rectangular, and indoor versus outdoor deployment, among others. All the analysis is backed by detailed experiments that are described in this paper.

INDEX TERMS Massive MIMO, precoding, testbed, user-pairing, Ls massive MIMO.

I. INTRODUCTION

Cellular connectivity became popular with the advent of 4G-Long Term Evolution (4G-LTE), a wireless standard that vastly improved connection speeds and reduced the price of connectivity per bit. The latest cellular standard 5G-New Radio (5G-NR) introduced by 3rd Generation Partnership Project (3GPP) [1], [2], [3], [4] is expected to accommodate immersive applications such as augmented and virtual reality with higher data rates, Internet of Things (IoT) applications like industrial monitoring, ultra-reliable and low latency services, mission-critical communications, automation, smart grid, etc. To meet the increased demands of cellular traffic and provide service to a massive number of devices, operators will be required to increase the network capacity of the existing cellular deployments. Massive Multiple Input Multiple Output (Massive MIMO) is considered as a key technology for 4G-LTE, 5G-NR and beyond 5G-NR cellular standards that have the potential to achieve such multi-fold improvements in the network capacity [5], [6], [7], [8], [9].

Massive MIMO is now a mainstream technology that is part of 4G-LTE, 5G-NR, and most certainly beyond 5G-NR cellular systems. It enabled substantial gains in spectral efficiency (SE) in wide area cellular networks [5], [6], [7], [8], [9]. The SE (SE) of 4G-LTE system with Massive MIMO is 3× the SE of a 4G-LTE system without Massive MIMO technology. In 5G-NR, a maximum of 12 orthogonal transmissions, i.e., 12 layers (12 spatial streams or 12 users) can be supported simultaneously on the same time-frequency resources, effectively supporting a 12× notional increase in

The associate editor coordinating the review of this manuscript and approving it for publication was Olutayo O. Oyerinde.

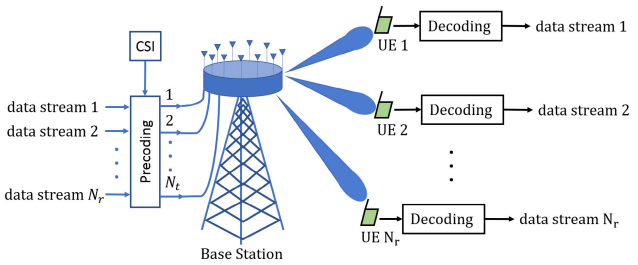

FIGURE 1. System model depicting downlink Massive MIMO.

SE. The next generation 6G standards are looking at the possible evolution of this Massive MIMO technology beyond the current capabilities.

The theoretical foundations of this Massive MIMO technology originate from the concepts of multiple data transmissions using multiple antennas initially proposed in [10]. Many advances have been made since then, eventually leading to understanding the Massive MIMO regime [11], [12], [13], [14]. With a large number of antennas at the base station (BS), the network operator can transmit the data to multiple user-equipments (UEs) on the same time-frequency resources and increase the network capacity [7] as shown in Fig. 1. In such a scenario, each UE suffers from inter-user interference, which degrades the received signal quality for each user. However, with various digital beamforming techniques [15], [16], [17], [18], [19], [20], this inter-user interference can be minimized, and an improvement in the network capacity can be achieved [21], [22]. In line of sight (LOS) conditions, the ability to support multiple such UEs is limited by the angular separation between the channel vectors of the UEs in both azimuth and elevation. This, in turn, depends on the spacing between the antenna elements of the antenna array at the BS. Thus, the physical size of the antenna array at the BS limits the user pairing capability. Further, in non line of sight (NLOS), theoretically, as many users as the number of antennas can be paired for the simultaneous transmissions when the channel vectors to each UE from the BS are independent and identically distributed (iid). However, the iid channel fading cannot be realized in practice, significantly impacting the user pairing and, thereby, the Massive MIMO performance. Though many theoretical models of Massive MIMO channel are available in the literature, practically achievable gains of Massive MIMO systems can only be understood through experiments. Few such existing testbed-based experiments mentioned in [23], [24], and [25] have quantified the achievable massive MIMO gains.

While theoretically, the behavior of MIMO has been understood over many years [5], [6], [7], [8], [9], in practice, many factors such as the size of the antenna array, spacing between antenna elements (in other words, the aperture of the antenna array), deployment considerations such as indoor vs. outdoor, the distance between the antenna array and the users, pilot contamination, etc. affect the performance of gains achieved by these MIMO and Massive MIMO systems. Despite these limitations, many systems have used some form of MIMO and Multiuser Multiple Input Multiple Output (MU-MIMO) concepts in practical deployments. Out of all these, TDD-based deployments play a significant role as the uplink channel can be used to identify the downlink channel, which can then be used to create interference-free transmissions to the users. This requires the users to be moving moderately slow so that there is enough density of pilots on the uplink to estimate the channels and relatively less interference from neighboring cells. Using such techniques, 5G-NR standards define 12-layer transmission using 12 orthogonal reference signal transmissions. For this to succeed, it is inherently assumed that the channel's frequency selectivity is relatively low. Therefore, precoding or beamforming calculation is done over the granularity of something known as Physical Resource Block (PRB) instead of on a subcarrier basis.

Various testbeds across industry and academia have evaluated the achievable gains with the MU-MIMO and Massive MIMO [26], [27], [28], [29], [30], [31], [32]. In [26], the Massive MIMO testbed at Lund University, in collaboration with the University of Bristol and National Instruments, considered 100 antenna ports at BS and has demonstrated 12 user-pairing on the same time-frequency resources using zero-forcing (ZF) precoder and maximum ratio transmission (MRT). In [27], the authors at Rice University and Bell labs have considered 64 antenna elements at the BS and have demonstrated 15 user-pairing with localized conjugate multiuser beamforming technique. In [28], with a Full-Dimension MIMO testbed, the authors at Samsung have demonstrated 12 user-pairing with 32 antenna ports at BS with signal-to-leakage and noise ratio (SLNR) precoding. However, the BSs developed in [26], [27], and [28] support a very limited sector for service. The limited area of service around the BS has a significant impact on the user-pairing, limiting it to 12, 15, 12 in [26], [27], and [28], respectively. In [29], the authors at Samsung Research America have demonstrated 7 user-pairing with 24 antenna ports (3 distributed antenna panel with each panel having 8 antenna ports). Although the distributed structure of the antenna array provides more coverage, the user-pairing capability demonstrated was limited. In [30], the authors at Fraunhofer Heinrich Hertz Institute demonstrated beamforming and interbeam interference removal using 32 antenna ports at BS. In [31], the authors at KU Leuven, Belgium, have demonstrated improvement in SE with real-time localization using 64 antenna ports at BS having various antenna array structures such as a uniform rectangular array, uniform linear array, distributed array, etc. However, the number of simultaneous users that can be paired in a real-time scenario has not been demonstrated in these testbeds [30], [31].

Despite all these efforts, the total achievable gain of Massive MIMO is not known in practical indoor or outdoor settings. While the standards limit to 12 layers, and in some cases, previously mentioned demonstrations have shown

TABLE 1. Comparison of our testbed implementation against the existing testbeds in the literature.

Testbed	LuMaMi	Argos	FD-MIMO	Modular Massive MIMO	Ls Massive MIMO
Institution	Lund University [26]	Rice University [27]	Samsung [28]	Samsung Research America [29]	IIT Hyderabad
Number of BS antenna ports	100	64	32	24	48
Number of BS antenna elements	50 (dual-polarized)	64	16 (dual-polarized)	12 (dual-polarized)	192 (co-polarized)
Antenna array structure at BS	Planar T-shaped	Rectangular	Rectangular	Rectangular distributed array	Circular
Carrier Frequency	3.7 GHz	2.4 GHz	3.5 GHz	3.5 GHz	2.36 GHz
Bandwidth	20 MHz	625 KHz	20 MHz	20 MHz	20 MHz
Transmit power per antenna port	NA	NA	18 dBm	18 dBm	20 dBm
Angular coverage around BS	Limited sector	Limited sector	Azimuth: 120^0, Elevation: 20^0	Large coverage	Azimuth: 360^0
Number of UEs served in DL	12	15	12	7	24

15 layers, no study shows the limits of such deployment in real settings. It is also not known if a sectored or circular deployment for a single-cell setup is optimal or not. Motivated by the details above, we evaluated the Massive MIMO performance in real-time for more than 15 user-pairing while considering different antenna structures at the BS. At IIT Hyderabad, we conducted a plethora of experiments to understand the fundamental limits of Massive MIMO in practical settings. The first set of results being presented in this paper is with a circular array with 48 antenna ports (192 antenna elements), where we show that simultaneously 24 layers, aka 24 users pairing each with a single layer, is achievable in an indoor setting. We refer to the usage of such a large antenna array to achieve a large number of user pairing on the same time-frequency resources as Large-scale Massive MIMO (Ls Massive MIMO) in this paper. Note that the real behavior is understood only via such experiments, and simulations are not enough to understand the real limits of such a technology. In the future, we will explore the behavior and performance of this Ls Massive MIMO testbed in outdoor settings, distributed settings such as cell-free MIMO, enhancing coverage using the massive arrays, and sweeping beams flexibly in 360^0 to handle multiple cell sites and many users.

In this paper, we present a first-of-its-kind Ls Massive MIMO testbed developed at IIT Hyderabad, where we have considered circular antenna array structure while evaluating the Massive MIMO behavior. We attempted simultaneous transmissions for 36 users using 48 antenna ports (where each antenna port has 4 elements in a 2×2 array). The evaluations are carried out in an indoor environment where there is a LOS component but strong reflections from multiple walls. Table 1 highlights the key differences of the Ls Massive MIMO testbed implementation compared with the existing testbed implementations in the literature. The key contributions of this testbed are summarized as follows.

- This is the first Massive MIMO testbed implementation that demonstrates as high as 24 user pairing in the same time-frequency resources. This high user pairing capability helps the network operators to support as many users in a limited amount of spectrum and achieve multifold improvement in the network capacity.
- To realize such massive gains, we have designed a user-pairing algorithm, where we calculate the correlation metric between the channel vectors of different UEs, select semi-orthogonal UEs based on this correlation metric, and perform ZF precoding for the paired users. In this work, we present in detail all the steps involved in the design, implementation, and validation of the proposed algorithm.
- We have evaluated the proposed user-pairing scheme using a circular antenna array of radius 1.524 m with 48 antenna ports (192 antenna elements) at BS and quantified the achievable gains with the proposed user-pairing scheme.
- Through extensive evaluations on the testbed in an indoor environment, we have shown that the proposed algorithm enables 24 user-pairing where each user data transmitted from BS has Quadrature Phase Shift Keying (QPSK) constellation. Additionally, we provide a detailed analysis of the user pairing behavior using Receiver Error Vector Magnitude (REVM) as a performance metric, where REVM is defined as the root mean square value of the error vector of the received modulation symbols. This metric clearly shows the impact of inter-user interference and the goodness of the precoding algorithms in an easy manner.

The remainder of this paper is organized as follows. Section II describes the testbed implementation, where we present the system architecture and the hardware components used in this testbed. In Section III, we propose the user pairing algorithm and explain the implementation of the

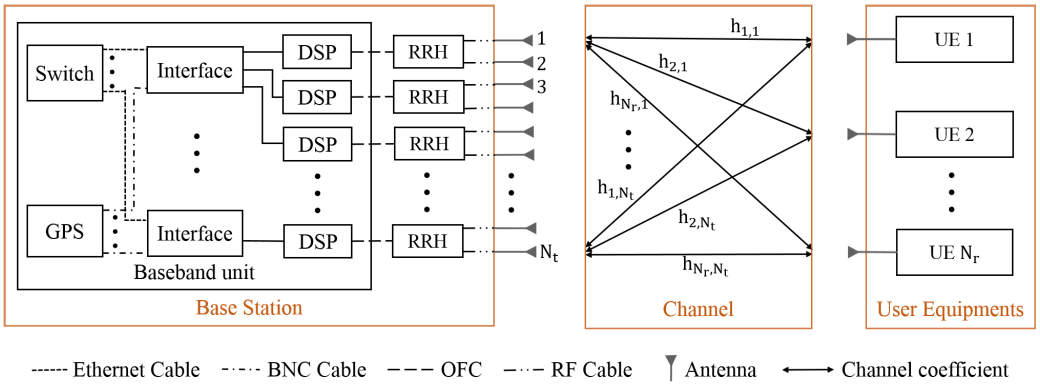

FIGURE 2. Design overview of the Large-scale Massive MIMO Testbed.

baseband algorithms in the testbed. Section IV presents the experimental setup and discusses the evaluation results from the testbed. In Section V, we provide concluding remarks and directions for future work.

Notation: $\mathbb{C}$, $\mathbb{R}$ denote the set of complex numbers and real numbers respectively; $\mathbb{E}\{.\}$ denotes the expectation of $\{.\}$; column vectors and matrices are denoted by lowercase and uppercase boldface letters, respectively; $\|a\|$ denotes the L2-norm of vector $\mathbf{a}$; $(.)^T$ and $(.)^H$ denotes the transpose and hermitian transpose of (.) respectively; $(.)^*$ denotes the complex conjugate of (.); $\langle a, b\rangle$ denotes the inner product of vectors $\mathbf{a}$ and $\mathbf{b}$, defined as $a^H b$ and $\boldsymbol{I}$ denotes the identity matrix of appropriate dimension.

II. TESTBED DESIGN

In this section, we present the design and implementation of the Ls Massive MIMO testbed. An overview of the testbed implementation has been presented in Fig. 2. BS consists of three key units namely, Baseband Unit (BBU), Remote Radio Head (RRH), and antenna array. The BBU performs all the baseband signal processing like user-pairing, precoding, modulation, Fast-Fourier transforms, etc. Digital Signal Processor (DSP) is the main component that carries out all such procedures. Since each DSP is designed to handle two parallel data streams, we rely on multiple DSPs connected to each other via a high-speed interface. Note that all these DSPs have their own independent clocks, and hence, to synchronize all of them, we use Global Positioning System (GPS) reference clock. Further, optical fiber cables (OFC) connects the BBU and RRH via the Common Public Radio Interface (CPRI) protocol. The main functionality of the RRH is to transmit and receive radio signals. In our testbed, we operate the RRH at an operating frequency of 2.36 GHz, the bandwidth of 20 MHz, and use Time Division Duplex (TDD) mode of transmissions. Note that it is configurable to use any Long Term Evolution (LTE) TDD frame structure as defined in 3GPP specifications [33] via ethernet ports.

The antenna array takes radio-frequency (RF) signal from RRH via RF cables and then radiates using the antenna elements into the wireless channel. In our testbed, we considered a circular antenna array. In Fig. 3, we present the design and the implementation of the circular antenna array. We consider the array radius to be 1.524 m at BS, placed at a height of 1.7 m as shown in Fig. 3a. Each antenna of this circular array has a single port and 4 antenna elements made up of microstrip patch (MSP). These 4 antenna elements are arranged in a 2×2 array with co-polarization and designed as per the principles outlined in [34]. Each antenna of this circular array has a width (w_a) and height (h_a) of 13.5 cm and 13.5 cm, respectively, whereas the width (w_p) and height (h_p) of each antenna element are 38 mm and 29.6 mm, respectively as shown in Fig. 3. The gain of each antenna element is 12 dBi with a 3 dB beamwidth of 50^0. We arranged 48 such single port antennas in a circle having a port-to-port distance (d_a) of 19 cm to form a circular array effectively with (48×4) 192 antenna elements, as shown in Fig. 3b. Further, this antenna array is designed with an operating frequency of 2.36 GHz. The antenna structure has a spacing of 2λ with an angular down tilt of 7.5^0, where λ is the wavelength of the electromagnetic wave radiated from the antenna. This structure covers the entire 360^0 area around BS in the azimuth direction and increases the user-pairing capability of BS on the same time-frequency resources.

We consider an omni-directional antenna with 5 dBi gain at each UE. The UEs in the testbed evaluation are physically separated with a distance of 0.91 m as shown in Fig. 3a. UEs numbered from 1 to 36 are arranged in a circle around the BS as shown in Fig. 3a, where each UE has a distance of 2.81 m from BS. This testbed setup is arranged in an indoor environment which has the dimensions of $8.96\text{ m} \times 8.14\text{ m} \times 3.58\text{ m}$, where there is a strong LOS and multiple reflections from concrete walls and roof.

III. PROPOSED BASEBAND ALGORITHMS

In this section, we first present the system model, and then we present the detailed explanation for Downlink (DL) Channel State Information (CSI) pilots, CSI estimation and feedback, UE pairing algorithm, linear precoder design,

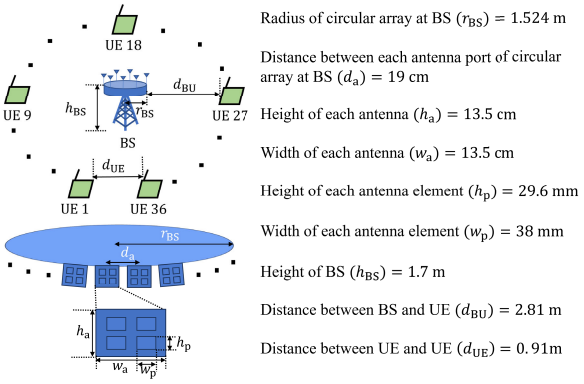

(a) Design of the circular arrangement

(b) Real-time implementation of the circular antenna array

FIGURE 3. Design and implementation of the circular antenna array.

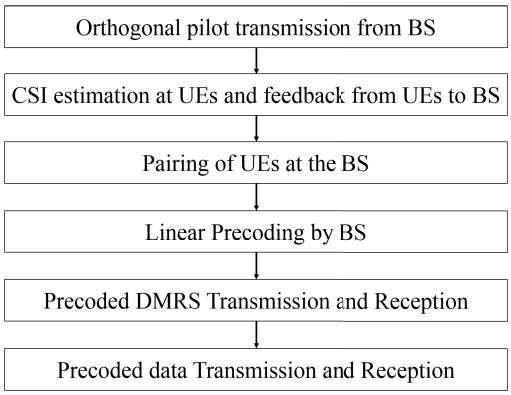

FIGURE 4. A brief description of proposed algorithm.

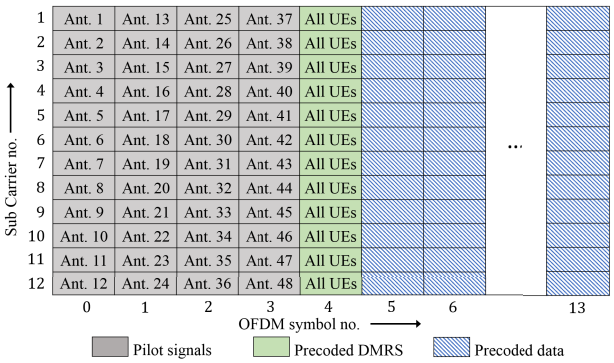

FIGURE 5. Time-Frequency grid for two PRBs (14 OFDM symbols and 12 subcarriers).

design of precoded Demodulation Reference Signal (DMRS), precoded data transmission and reception, and computational complexity of the proposed algorithms.

In this testbed, we consider the downlink Massive MIMO system as shown in Fig. 1, where a BS equipped with the massive number of antennas communicates with the multiple UEs on the same-time frequency resources. At BS, we consider N_t as the number of antenna ports where each port effectively is a combination of multiple antenna elements. We then consider N_r number of physically separated UEs where each UE has a single antenna. Further, we denote $\boldsymbol{s} = [s_1, s_2, \ldots, s_{N_r}]^T \in \mathbb{C}^{N_r}$ as the data stream vector, where each element $s_i \in \mathbb{C}$ represents the modulated data symbol satisfying unit power, i.e., $\mathbb{E}\{s_i s_i^H\} = 1$. Prior to the transmission in the downlink, this data stream vector $\boldsymbol{s}$ is precoded with a precoder matrix $\boldsymbol{W} \in \mathbb{C}^{N_t \times N_r}$. Thus, we have the effective transmitted signal from the BS as $\boldsymbol{x} = \boldsymbol{W}\boldsymbol{s}$, where $\boldsymbol{x} = [x_1, x_2, \ldots, x_{N_t}]^T \in \mathbb{C}^{N_t}$ with each element $x_j \in \mathbb{C}$ represents the transmitted signal from BS antenna port j.

The MIMO channel matrix between the BS and UEs is denoted as $\boldsymbol{H} \in \mathbb{C}^{N_r \times N_t}$, where each element $h_{i,j}$ is the channel coefficient between BS antenna port j and UE i. Hence, the received signal vector for all UEs is formulated as follows.

$$\begin{aligned} \boldsymbol{y} &= \boldsymbol{H}\boldsymbol{x} + \boldsymbol{n}, \\ &= \boldsymbol{H}\boldsymbol{W}\boldsymbol{s} + \boldsymbol{n}, \end{aligned}$$

where, $\boldsymbol{y} = [y_1, y_2, \ldots, y_{N_r}]^T \in \mathbb{C}^{N_r}$ with element $y_i \in \mathbb{C}$ denotes the received signal at UE i for $1 \leq i \leq N_r$ and $\boldsymbol{n} = [n_1, n_2, \ldots, n_{N_r}]^T \in \mathbb{C}^{N_r}$ is noise vector corresponding to all UEs. We consider that these channel coefficients are estimated at each UE and are feedback to the BS. Thus, the BS can construct the entire channel matrix $\boldsymbol{H}$ and generate the appropriate precoder matrix $\boldsymbol{W}$. The precoder matrix $\boldsymbol{W}$ has a significant role in enabling the BS to communicate with multiple UEs on the same time-frequency resources by mitigating inter-user interference. We present a brief overview of this design in Fig. 4, and a detailed explanation of each block is presented next.

A. ORTHOGONAL PILOT TRANSMISSION FROM BS

To implement Massive MIMO in real-time, BS needs CSI, using which it performs the precoding operation. In 3GPP LTE and NR, the BS use sounding reference signal (SRS) transmitted in Uplink (UL) for CSI estimation [1], [2]. In our experiment, we approximate the SRS-based implementation procedures using explicit CSI pilot signals in DL, where BS

transmits known pilot signals so that UE can estimate the CSI and feedback them to the BS. However, for the CSI to be of good quality, we allow the BS to orthogonally transmit the pilot signals from different antenna ports, as shown in Fig. 5, where we have named the 48 BS antenna ports as Ant. 1 to Ant. 48. Then, the pilot signal is transmitted once on a resource element (RE) per BS antenna port per PRB, which is received by all the UEs. The UEs use these received pilot signals for CSI estimation. Note that the CSI estimated in the current subframe is used to precode the DMRS and data transmitted in the next subframe, and this procedure is repeated across time. Next, we explain in detail the CSI estimation procedure.

B. CSI ESTIMATION AT UES AND FEEDBACK FROM UES TO BS

On the RE assigned for pilot signals, each UE estimates their CSI using the pilot signals with least square (LS) estimation. After CSI estimation, all UEs feedback the CSI to the BS. Hence, the DL CSI matrix $\boldsymbol{H}$ is constructed at BS after receiving CSI feedback from all UEs as shown below

$$\boldsymbol{H} = \begin{bmatrix} h_{1,1} & h_{1,2} & h_{1,3} & \ldots\ldots\ldots & h_{1,N_\mathrm{t}} \\ h_{2,1} & h_{2,2} & h_{2,3} & \ldots\ldots\ldots & h_{2,N_\mathrm{t}} \\ \vdots & \vdots & \vdots & \ldots\ldots\ldots & \vdots \\ \vdots & \vdots & \vdots & \ldots\ldots\ldots & \vdots \\ h_{N_\mathrm{r},1} & h_{N_\mathrm{r},2} & h_{N_\mathrm{r},3} & \ldots\ldots\ldots & h_{N_\mathrm{r},N_\mathrm{t}} \end{bmatrix} \tag{1}$$

where each row corresponds to UE i and each column corresponds to BS antenna port j and $h_{i,j}$ is the channel coefficient between BS antenna port j and UE i. We denote the i^{th} row of matrix $\boldsymbol{H}$ shown in (1) as $(\hat{\boldsymbol{h}}_i)^T$, where $(\hat{\boldsymbol{h}}_i) = [h_{i,1}, h_{i,2}, h_{i,3}, \ldots, h_{i,N_\mathrm{t}}]^T \in \mathbb{C}^{N_\mathrm{t}}$ is a channel vector corresponding to UE i. Now, we formulate channel matrix as $\boldsymbol{H} = [(\hat{\boldsymbol{h}}_1)\ (\hat{\boldsymbol{h}}_2)\ \ldots\ (\hat{\boldsymbol{h}}_{N_\mathrm{r}})]^T$. The first row of channel matrix $\boldsymbol{H}$ is feedback from UE 1, the second row is feedback from UE 2, and so on till UE N_r. Now, given the CSI matrix, the BS has to perform the precoding operation before transmitting in DL. However, before precoding, we need to select spatially well-separated users out of the N_r UEs. For this, we propose a user pairing algorithm, which will be explained next.

C. PROPOSED USER PAIRING ALGORITHM

Since all UEs are spatially distributed, the CSI obtained from various UEs are at different power scales due to the effect of different path losses observed by the UEs. For the BS to do the precoding, the CSI received from all the UEs must be on a similar power scale. Hence, we normalize the channel vector coming from each UE, and then we form a new CSI matrix denoted as $\boldsymbol{H}_1 \in \mathbb{C}^{N_\mathrm{r} \times N_\mathrm{t}}$. To achieve this normalization, we divide each row of channel matrix $\boldsymbol{H}$ with their L2-norm.

$$\boldsymbol{H}_1 = \begin{bmatrix} \tilde{h}_{1,1} & \tilde{h}_{1,2} & \tilde{h}_{1,3} & \ldots\ldots\ldots & \tilde{h}_{1,N_\mathrm{t}} \\ \tilde{h}_{2,1} & \tilde{h}_{2,2} & \tilde{h}_{2,3} & \ldots\ldots\ldots & \tilde{h}_{2,N_\mathrm{t}} \\ \vdots & \vdots & \vdots & \ldots\ldots\ldots & \vdots \\ \vdots & \vdots & \vdots & \ldots\ldots\ldots & \vdots \\ \tilde{h}_{N_\mathrm{r},1} & \tilde{h}_{N_\mathrm{r},2} & \tilde{h}_{N_\mathrm{r},3} & \ldots\ldots\ldots & \tilde{h}_{N_\mathrm{r},N_\mathrm{t}} \end{bmatrix} \tag{2}$$

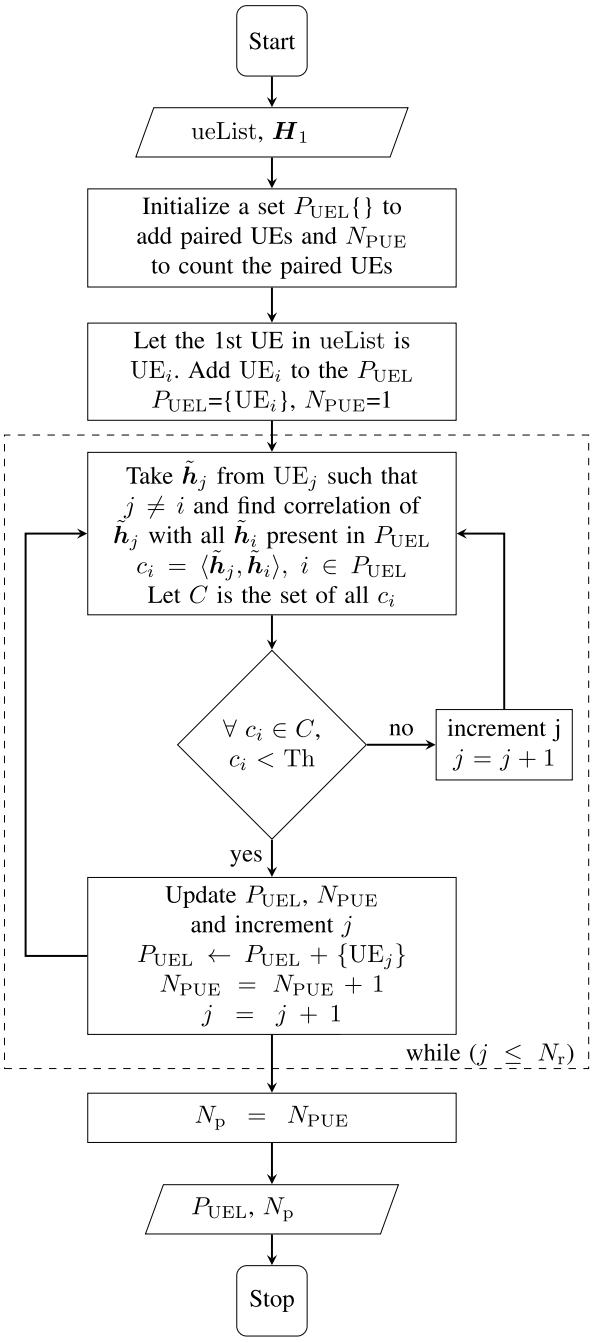

FIGURE 6. Proposed user pairing algorithm.

where $\tilde{h}_{i,j} = \frac{h_{i,j}}{\|(\hat{\boldsymbol{h}}_i)^T\|}$, $1 \leq i \leq N_\mathrm{r}, 1 \leq j \leq N_\mathrm{t}$, $\|(\hat{\boldsymbol{h}}_i)^T\|$ is L2-norm of channel vector of UE i. Now, the normalized channel matrix presented in (2) can be written as $\boldsymbol{H}_1 = [(\tilde{\boldsymbol{h}}_1)\ (\tilde{\boldsymbol{h}}_2)\ \ldots\ (\tilde{\boldsymbol{h}}_{N_\mathrm{r}})]^T$, where $(\tilde{\boldsymbol{h}}_i) = [\tilde{h}_{i,1}, \tilde{h}_{i,2}, \tilde{h}_{i,3}, \ldots, \tilde{h}_{i,N_\mathrm{t}}]^T \in \mathbb{C}^{N_\mathrm{t}}$ is normalized channel vector corresponding to UE i, $1 \leq i \leq N_\mathrm{r}$.

To spatially multiplex the UEs, we use linear precoding, where we perform the pseudo inverse of the CSI matrix. For pseudo inverse, the rows of the CSI matrix should be linearly independent. However, we achieve the maximum gains with spatial multiplexing when the channel vectors of

the users are orthogonal [19]. This is not always achievable in practice. Hence, we consider the users whose channel vectors are semi-orthogonal in the proposed algorithm. For this, we calculate the correlation between the channel vectors of UEs and ensure that it is less than a predefined threshold value as follows. We denote the list of all the active UEs as ueList $= \{1, 2, 3, \ldots, N_r\}$. Then, we select one UE from the ueList and add it to a new list called P_{UEL}. We pick the second UE from ueList and perform a correlation check between the channel vector of the first and second UE. Now, if this correlation value is less than a predefined threshold (Th), we add this second UE to P_{UEL} otherwise, we discard this UE for scheduling in the current subframe. Then, we take the third UE from ueList and perform a correlation check with all the UEs present in P_{UEL}. If all the evaluated correlation values are less than a predefined Th, we add the third UE to P_{UEL}. This procedure is repeated for all the active UEs present in ueList. We have presented in detail the proposed user pairing algorithm in Fig. 6. Next, we explain the precoding procedure for the paired users.

D. LINEAR PRECODER

Given a list of the paired UEs denoted as P_{UEL}, the number of paired UEs N_p ($N_p \leq N_r$), and the number of BS antenna ports (N_t), we construct a new CSI matrix denoted as $\boldsymbol{H}_2 \in \mathbb{C}^{N_p \times N_t}$. Note that this $\boldsymbol{H}_2$ is formulated using only the paired users picked from the active users. While constructing the precoder matrix, the BS performs the pseudo inverse of new CSI matrix $\boldsymbol{H}_2$ to cancel the inter-user interference as shown in Fig. 6. Hence, the precoder matrix $\boldsymbol{W}_p \in \mathbb{C}^{N_t \times N_p}$ is expressed as follows.

$$\boldsymbol{W}_p = \boldsymbol{H}_2^H (\boldsymbol{H}_2 \boldsymbol{H}_2^H)^{-1}, \tag{3}$$

After generating the precoder matrix $\boldsymbol{W}_p$ as per (3), we then precode the DMRS and data for the downlink transmission.

E. PRECODED DMRS TRANSMISSION AND RECEPTION

We denote the propagation CSI matrix experienced by paired UEs as $\boldsymbol{H}_p \in \mathbb{C}^{N_p \times N_t}$ whose rows are the channel vectors of paired UEs. Theoretically, if $\boldsymbol{W}_p$ is pseudo inverse of $\boldsymbol{H}_p$ then $\boldsymbol{H}_p \boldsymbol{W}_p = \boldsymbol{I}$. But in practice, the CSI cannot be estimated per tone due to the pilot overhead as it is computationally complex and significant pilot overhead to estimate CSI per tone. Therefore, per PRB, precoding is used, which results in performance losses leading to inter-user interference in the presence of a frequency-selective channel. Also, such a performance loss only increases as the number of paired users increases. Also, since instantaneous CSI is not possible, we need to use the channel estimated from the previous subframes to precode the data transmitted in the current subframe. Due to these reasons, in practice, we observe that $\boldsymbol{H}_p \boldsymbol{W}_p \neq \boldsymbol{I}$.

For the UEs to decode the precoded data, the BS transmits DMRS with the same precoding as that is used for the data transmission. Thus, when the DMRS vector $\boldsymbol{s}_{dm} \in \mathbb{C}^{N_p}$ is precoded with $\boldsymbol{W}_p$, it results in $\boldsymbol{x}_{dm} \in \mathbb{C}^{N_t}$, as shown below.

$$\boldsymbol{x}_{dm} = \boldsymbol{W}_p \, \boldsymbol{s}_{dm},$$

where, $\boldsymbol{s}_{dm} = [(s_{dm})_1, (s_{dm})_2, \ldots, (s_{dm})_{N_p}]^T$, whose i^{th} element $(s_{dm})_i \in \mathbb{C}$ represents the transmitted DMRS for UE i, $i \in P_{UEL}$. The implementation of the precoded DMRS vector transmission per RE is presented in Fig. 5.

The received DMRS vector $\boldsymbol{y}_{dm} \in \mathbb{C}^{N_p}$ for all UEs on each RE is formulated as follows.

$$\boldsymbol{y}_{dm} = \boldsymbol{H}_p \, \boldsymbol{x}_{dm} + \boldsymbol{n}, \tag{4}$$

where, $\boldsymbol{y}_{dm} = [(y_{dm})_1, (y_{dm})_2, \ldots, (y_{dm})_{N_p}]^T$, whose i^{th} element $(y_{dm})_i \in \mathbb{C}$ represents the received DMRS at UE i. Since precoding cancels the inter-user interference, each UE receives its DMRS with minimal interference as per (4). Now, using this received DMRS, we estimate the precoded CSI ($\hat{e}_i \in \mathbb{C}$) for UE i on all subcarriers as shown below.

$$\hat{e}_i = \frac{((s_{dm})_i)^* \cdot (y_{dm})_i}{|(s_{dm})_i|^2}, \; i \in P_{UEL}, \tag{5}$$

Next, we explain the data transmission, equalization, and decoding of the received data in detail.

F. DATA TRANSMISSION AND RECEPTION

We precode the data vector $\boldsymbol{s}_d \in \mathbb{C}^{N_p}$ to generate the precoded data vector $\boldsymbol{x}_d \in \mathbb{C}^{N_t}$ as shown below.

$$\boldsymbol{x}_d = \boldsymbol{W}_p \, \boldsymbol{s}_d,$$

where $\boldsymbol{s}_d$ is the vector of digital modulated symbols, for example, QPSK, 16QAM, and 64QAM. Further, $(s_d)_i \in \mathbb{C}$ is i^{th} element of $\boldsymbol{s}_d$ where $i \in P_{UEL}$ and it represents the data for UE i. Then, we transmit this precoded data vector on each RE allocated for data transmission as shown in Fig. 5. The received data vector $\boldsymbol{y}_d \in \mathbb{C}^{N_p}$ for all UEs on each RE is formulated below.

$$\boldsymbol{y}_d = \boldsymbol{H}_p \, \boldsymbol{x}_d + \boldsymbol{n}, \tag{6}$$

where, $\boldsymbol{y}_d = [(y_d)_1, (y_d)_2, \ldots, (y_d)_{N_p}]^T$, whose i^{th} element $(y_d)_i \in \mathbb{C}$ represents the received data at UE i. Since precoding cancels the inter-user interference, each UE receives its data with minimal interference as per (6). We use the ($\hat{e}_i$) explained earlier in (5) to equalize the received data $(y_d)_i$ for UE i on each RE as shown below.

$$(\hat{s}_d)_i = \frac{(\hat{e}_i)^* \cdot (y_d)_i}{|\hat{e}_i|^2}, \; i \in P_{UEL}, \tag{7}$$

where, $(\hat{s}_d)_i \in \mathbb{C}$ is the equalized data for UE i on each RE. This equalized data from (7) is then used for further baseband processing like demodulation, REVM measurement, etc. Next, we present the steps involved in the experimental evaluation and discuss the results in detail.

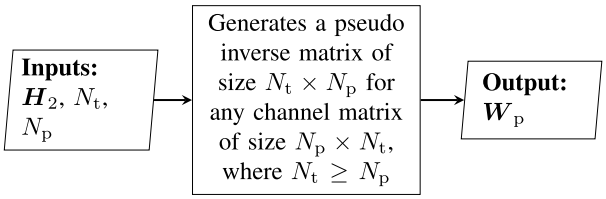

FIGURE 7. Pseudo inverse operation.

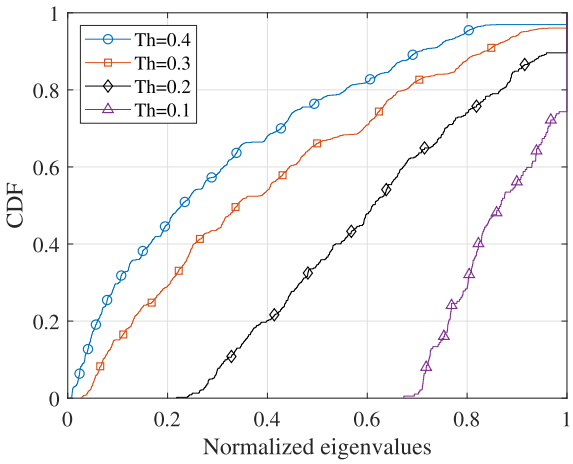

FIGURE 8. CDF plot of normalized eigenvalues of ($H_2H_2^H$) matrix.

G. COMPLEXITY EVALUATION OF PROPOSED ALGORITHM

The proposed user-pairing algorithm in the previous section is based on the correlation between the channel vectors of all UEs. To find the correlation between channel vectors of 2 different UEs, we use the dot product of complex vectors, which consumes 4 multiplications for each complex multiplication, and thus it requires $4N_t$ multiplications to check the correlation between two UE channel vectors, where N_t is the number of antennas at BS. Further, it requires 2 additions for each complex multiplication, hence $2N_t$ additions for N_t complex multiplication. By considering the real and imaginary parts separately while performing addition, we need $2(N_t - 1)$ computations for N_t complex numbers. Hence, in total, we require $(2N_t + 2N_t - 2) = (4N_t - 2)$ additions and $4N_t$ multiplications for computing the correlation of channel vectors between two UEs. In the worst-case scenario, when all N_r UEs are paired, the maximum number of correlation checks required is $\frac{N_r(N_r-1)}{2}$.

IV. EXPERIMENT RESULTS

In this section, we first present the real-time DL CSI analysis, the impact of correlation threshold on UE pairing, and REVM analysis of the received signals. Then, we present the real-time experiment results captured from the testbed in different experiments where we present the DL received constellation, the REVM of received data for all paired UEs with different modulation schemes, and correlation thresholds.

A. DL CSI ANALYSIS

We perform the evaluation of the testbed in an indoor environment with an approximate dimension of the room being 8.96 m × 8.14 m × 3.58 m. From this experiment, we recorded the real-time DL CSI matrices for different experiments. Further, we analyzed the eigenvalues of these DL CSI matrices for various experiments with different correlation Th. Depending on the value of Th, the number of paired UEs changes, and so the size of CSI matrix changes after pairing. Thus, the size of ($\boldsymbol{H}_2\boldsymbol{H}_2^H$) is also different for various Th values. We analyze the eigenvalues of ($\boldsymbol{H}_2\boldsymbol{H}_2^H$) for various Th values. For this purpose, we perform the eigenvalue decomposition of ($\boldsymbol{H}_2\boldsymbol{H}_2^H$) as follows.

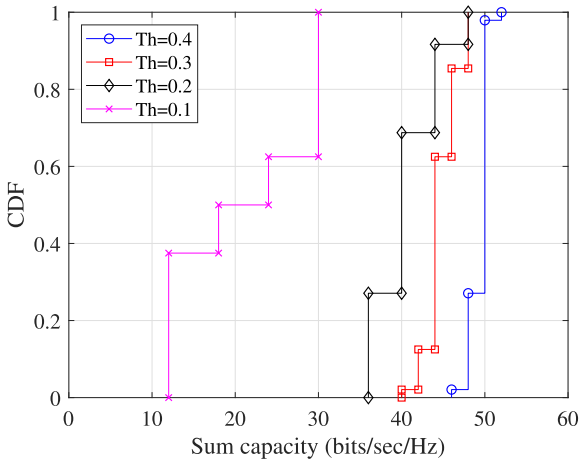

FIGURE 9. CDF plot of sum capacity in bits/sec/Hz.

$$\boldsymbol{A} = \boldsymbol{U}\Lambda\boldsymbol{U}^H, \tag{8}$$

where $\boldsymbol{A} = \boldsymbol{H}_2\boldsymbol{H}_2^H \in \mathbb{C}^{N_p \times N_p}$ is a square matrix, $\Lambda = diag(\lambda_1, \lambda_2, \ldots, \lambda_{N_p}) \in \mathbb{R}^{N_p \times N_p}$ is a diagonal matrix whose diagonal elements are eigenvalues of $\boldsymbol{A}$, $\boldsymbol{U} = [\boldsymbol{u}_1, \boldsymbol{u}_2, \ldots, \boldsymbol{u}_{N_p}] \in \mathbb{C}^{N_p \times N_p}$ is a unitary matrix whose j^{th} column vector ($\boldsymbol{u}_j$) is a eigen vector of $\boldsymbol{A}$ coresponding to eigenvalue λ_j, $1 \leq j \leq N_p$. Note that the received signal strength at the UEs is proportional to the normalized eigenvalues of ($\boldsymbol{H}_2\boldsymbol{H}_2^H$), i.e., the larger the normalized eigenvalues, the better will be the signal to interference plus noise ratio (SINR). Hence, we have computed the normalized eigenvalues of ($\boldsymbol{H}_2\boldsymbol{H}_2^H$) and plotted the cumulative distribution function (CDF) of these normalized eigenvalues in Fig. 7.

As shown in Fig. 7, we have considered various Th values. Note that CSI matrix $\boldsymbol{H}$ has size 36 × 48, but after pairing the size of new CSI matrix $\boldsymbol{H}_2$ is N_p × 48 where the number of paired UEs (N_p) depends on the value of Th. As the Th value decreases, the BS discards the UEs, which have a correlated channel, and thus, improves the performance for the remaining paired UEs. Hence, as shown in Fig. 7, the normalized eigenvalues are larger for smaller Th values, which in turn improve the SINR of the user.

We have calculated the channel sum capacity while evaluating the algorithm in our testbed as follows.

$$\boldsymbol{C} = \sum_{k=1}^{K} (N_k n_k), \tag{9}$$

TABLE 2. Testbed parameters for different experiments.

Parameters	Expt-1	Expt-2	Expt-3	Expt-4
Number of BS antenna ports (N_t)	48	48	48	48
Number of BS antenna elements	192 (co-pol)	192 (co-pol)	192 (co-pol)	192 (co-pol)
BS antenna array type	Circular	Circular	Circular	Circular
Total number of UEs (N_r)	36	36	36	36
Correlation threshold (Th)	0.3	0.1	0.1	0.1
Modulation scheme	QPSK	QPSK	16QAM	64QAM
Total Tx power from BS	36.8 dBm			
Tx power per antenna port	20 dBm			
Rx sensitivity per antenna port	−70 dBm to −90 dBm			

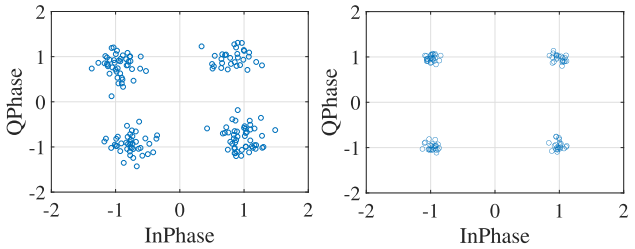

(a) UE 22 (Th = 0.4) (b) UE 22 (Th = 0.3)

FIGURE 10. Comparision of constellation for different correlation thresholds for a given UE.

TABLE 3. Number of paired UEs for different correlation thresholds.

Correlation threshold (Th)	Maximum number of paired UEs in a radio frame	Minimum number of paired UEs in a radio frame
0.1	5	3
0.2	12	7
0.3	24	20
0.4	36	31

where $\boldsymbol{C}$ is the channel sum capacity, N_k is the number of paired UEs decoded the data with k^{th} modulation scheme which gives a data rate of n_k bits per second per Hz. Further, $\sum_{k=1}^{K}(N_k) = N_p$, where K is the total number of modulation schemes and N_p is the total number of users paired. Note that for various correlation threshold (Th) values, the number of paired UEs (N_p) varies. Thus, the achieved channel sum capacity varies with different Th values. Fig. 10 presents CDF of channel sum capacity for different Th values ranging from 0.1 to 0.4. As shown in Fig. 8, the achievable gain saturates with an increase in the Th values, as beyond certain pairing, the inter-user interference dominates, and the achievable gains saturate.

We present a comparison of the received constellation for a given UE (UE 21) for different Th values in Fig. 11. We observe that the constellation of the received signal is significantly better in the case of Th $=$ 0.3 as compared to Th $=$ 0.4. This behavior aligns with our assumption that by decreasing the Th value, there will be an improvement in the SINRs observed by each paired user. In our lab (indoor environment), we can observe clear received constellations in DL for Th values less than or equal to 0.3. Next, we provide a detailed analysis of UE pairing for different values of Th.

B. SIGNIFICANCE OF CORRELATION THRESHOLD FOR UE PAIRING

To analyze the impact of the correlation threshold on the number of UEs paired by BS, we have evaluated for different correlation Th values such as 0.1, 0.2, 0.3, etc. In Table 3, we present the number of paired UEs for different correlation Th values in a given radio frame. From Table 3, given a fixed number of BS antennas, with an increase in Th, we observe that there is an increase in the number of UEs paired. However, from Fig. 10, the received constellations become much scattered with the increase in Th. Hence, the BS has to appropriately choose the Th value for optimal performance. Further, to quantify this scattering observed in the constellations, next, we define a metric called REVM and provide a detailed analysis of the same.

C. REVM AS A PERFORMANCE METRIC

In [35], the 3GPP standards define the transmitter Error Vector Magnitude (EVM) for measuring the signal quality. In our experiment, we use the EVM measured at the receiver called REVM to determine the quality of the received signal. REVM is defined as the root mean square (RMS) value of error vector $\boldsymbol{e}_{\text{err}} \in \mathbb{R}^2$ for a number of N randomly transmitted digital modulation symbols [36], [37]. The RMS and percentage value of REVM can be expressed as

$$\text{REVM}_{\text{RMS}} = \sqrt{\frac{\frac{1}{N}\sum_{i=1}^{N}|\boldsymbol{e}_{\text{err},i}|^2}{|\boldsymbol{e}_{\text{t,a}}|^2}},$$
$$\%\text{REVM} = \text{REVM}_{\text{RMS}} \times 100, \tag{10}$$

TABLE 4. Paired UE numbers for all experiments.

Radio Frame	Expt-1		Expt-2		Expt-3		Expt-4	
	N_{p}	P_{UEL}	N_{p}	P_{UEL}	N_{p}	P_{UEL}	N_{p}	P_{UEL}
1	20	1, 2, 3, 5, 8, 9, 10, 11, 12, 15, 16, 18, 22, 25, 29, 31, 32, 33, 34, 35	3	1, 6, 7	3	1, 6, 8	3	1, 4, 6
2	21	1, 2, 3, 5, 8, 9, 10, 11, 12, 15, 16, 18, 22, 25, 29, 31, 32, 33, 34, 35, 36	4	1, 6, 7, 34	4	1, 7, 11, 25	3	1, 6, 15
3	22	1, 2, 4, 5, 8, 9, 10, 11, 12, 15, 16, 18, 19, 22, 25, 29, 31, 32, 33, 34, 35, 36	4	1, 6, 9, 33	4	1, 4, 5, 25	4	1, 4, 9, 11
4	23	1, 2, 3, 4, 5, 8, 9, 10, 11, 12, 15, 16, 18, 22, 23, 25, 29, 31, 32, 33, 34, 35, 36	5	1, 6, 16, 22, 34	5	1, 4, 9, 11, 25	5	1, 4, 6, 9, 11
5	24	1, 2, 3, 4, 5, 8, 9, 10, 11, 12, 15, 16, 18, 19, 22, 23, 25, 29, 31, 32, 33, 34, 35, 36	5	1, 6, 13, 16, 34	5	1, 4, 7, 11, 25	5	1, 4, 6, 11, 15

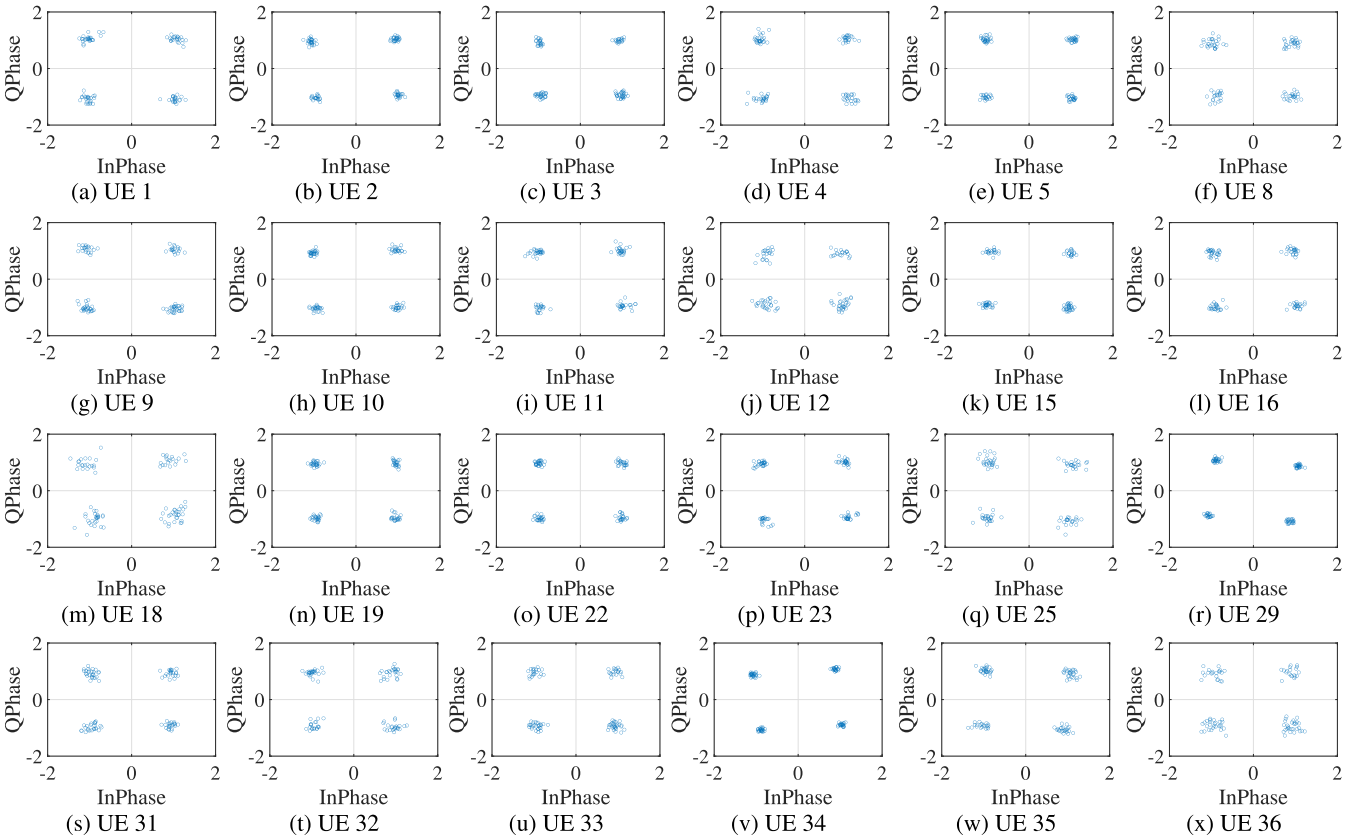

FIGURE 11. Downlink received constellation diagrams for Expt-1.

where, $\boldsymbol{e}_{\mathrm{err},i} = \boldsymbol{e}_{\mathrm{r},i} - \boldsymbol{e}_{\mathrm{t},i}$, $|\boldsymbol{e}_{\mathrm{t,a}}|^2 = \frac{1}{M}\sum_{i=1}^{M}|\boldsymbol{e}_{\mathrm{t},i}|^2$, $\boldsymbol{e}_{\mathrm{err},i}$ is i^{th} error vector, $\boldsymbol{e}_{\mathrm{r},i}$ is i^{th} received signal vector, $\boldsymbol{e}_{\mathrm{t},i}$ is i^{th} transmitted signal vector, $|\boldsymbol{e}_{\mathrm{t,a}}|^2$ is the average power of all M symbols within a constellation, M is the number of symbols in a constellation set. The calculation used for formulating the REVM is shown in (10). Note that the target transmitter EVM mentioned by 3GPP for QPSK, 16QAM, and 64QAM is 17.5%, 12.5%, and 8% respectively [35], whereas REVM can be comparatively higher.

In Table 2, we present the various testbed parameters considered in different experiments. Next, we present in detail the results on the number of UEs being paired for various Th values along with their corresponding received constellations and REVM values.

D. EXPERIMENTS

1) EXPT-1

In this experiment, we have considered 48 BS antennas arranged in a circular array as shown in Fig. 3b, 36 UEs are arranged in a circle around BS as shown in Fig. 3a, correlation Th has been set to 0.3, and data stream for all UEs has been set to QPSK modulation. As per the channel conditions observed in practice, our proposed pairing algorithm selects different

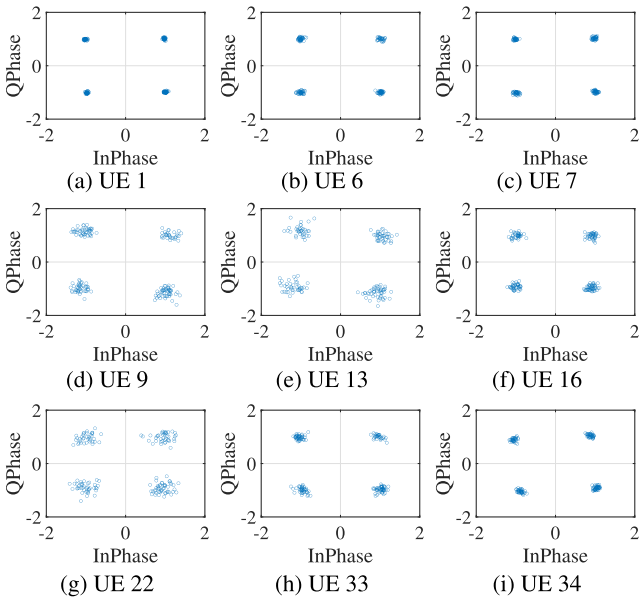

FIGURE 12. Downlink received constellation diagrams for Expt-2.

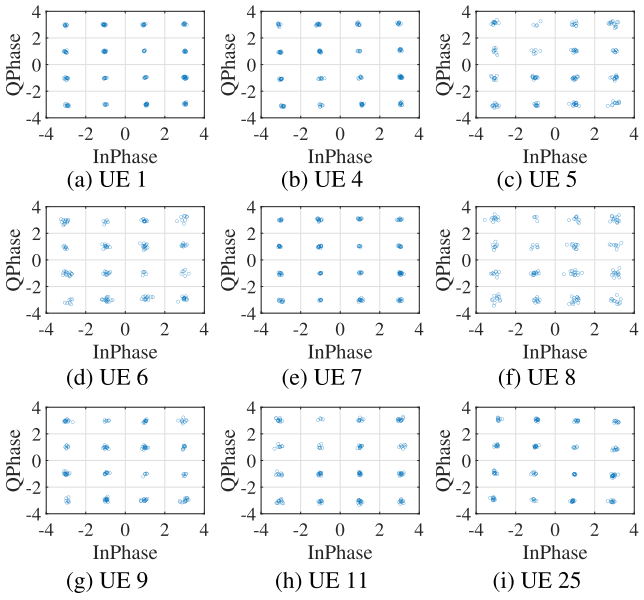

FIGURE 13. Downlink received constellation diagrams for Expt-3.

UEs in various radio frames based on the correlation metric chosen. Thus, the UEs being paired is different across various radio frames.

In Table 4, we have captured the real-time data of N_p and P_{UEL} for various radio frames. As shown in Table 4, for the current scenario, a maximum of 24 and a minimum of 20 UEs are paired out of 36 UEs in one radio frame. In Fig. 12, we present the received QPSK constellations at all paired UEs captured in the radio frame where 24 UEs are paired.

We have also formulated the REVM measurement from the testbed and presented it in Table 5. For the UEs that are not paired in the radio frame, we have denoted 'NA' for % REVM. We observe that for the current experiment, 10 UEs have REVM in between 0% to 10%, 14 UEs have REVM in between 10% to 20% as shown in Table 6.

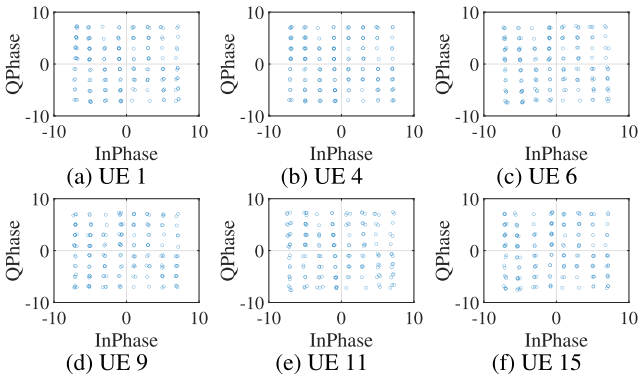

FIGURE 14. Downlink received constellation diagrams for Expt-4.

2) EXPT-2

In this experiment, we have considered 48 BS antennas arranged in a circular array as shown in Fig. 3b, 36 UEs are arranged in a circle around BS as shown in Fig. 3a, correlation Th has been set to 0.1, and data stream for all UEs has been set to QPSK modulation.

As shown in Table 4, for the current experiment, a maximum of 5 and a minimum of 3 UEs are paired out of 36 UEs in one radio frame. The received QPSK constellations of all paired UEs are shown in Fig. 13. From Table 5, we observe that for the current experiment, 6 UEs have REVM in between 0% to 10%, 3 UEs have REVM in between 10% to 20% as shown in Table 6.

3) EXPT-3

In this experiment, we have considered 48 BS antennas arranged in a circular array as shown in Fig. 3b, 36 UEs are arranged in a circle around BS as shown in Fig. 3a, correlation Th has been set to 0.1 and data stream for all UEs has been set to 16QAM modulation.

From Table 4, we observe that for the current experiment, a maximum of 5 and a minimum of 3 UEs are paired out of 36 UEs in one radio frame. The received 16QAM constellations of all paired UEs are shown in Fig. 14. The REVM measurements for the current experiment captured from the testbed are presented in Table 5, where We observe that all 9 UEs have REVM in between 0% to 10%.

4) EXPT-4

In this experiment, we have considered 48 BS antennas arranged in a circular array as shown in Fig. 3b, 36 UEs are arranged in a circle around BS as shown in Fig. 3a, correlation Th has been set to 0.1 and data stream for all UEs has been set to 64QAM modulation.

As shown in Table 4 for the current experiment, a maximum of 5 and a minimum of 3 UEs are paired out of 36 UEs in one radio frame. The received 64QAM constellations of all paired UEs are shown in Fig. 14. Table 5 presents the REVM measurements for the current experiment captured from the testbed. We observe that for the current experiment, all 6 UEs have REVM in between 0% to 10%.

TABLE 5. REVM of all paired UEs for all experiments.

Expt-1						Expt-2		Expt-3		Expt-4	
UE	%REVM	UE	%REVM	UE	%REVM	UE	%REVM	UE	%REVM	UE	%REVM
1	12.14	13	NA	25	14.64	1	2.98	1	2.74	1	2.78
2	8.36	14	NA	26	NA	6	4.61	4	3.80	4	1.79
3	9.03	15	9.75	27	NA	7	4.38	5	5.22	6	3.59
4	12.10	16	11.04	28	NA	9	17.05	6	6.08	9	2.93
5	7.56	17	NA	29	11.59	13	20.32	7	3.03	11	4.40
6	NA	18	19.69	30	NA	16	10.37	8	7.21	15	4.27
7	NA	19	8.75	31	12.61	22	18.11	9	4.13		
8	14.45	20	NA	32	13.80	33	9.28	11	4.66		
9	11.31	21	NA	33	11.56	34	9.98	25	4.93		
10	8.50	22	7.75	34	10.64						
11	10.58	23	9.92	35	12.20						
12	17.11	24	NA	36	16.95						

TABLE 6. Observation for all experiments.

	%REVM **Range**	**Number of UEs**
Expt-1	0% to 10%	10
	10% to 20%	14
Expt-2	0% to 10%	6
	10% to 20%	3
Expt-3	0% to 10%	9
Expt-4	0% to 5%	6

V. CONCLUSION AND FUTURE WORK

In this paper, we presented the Ls Massive MIMO testbed at IIT Hyderabad, which is a fully operational real-time testbed that demonstrates the realization of high network capacities achievable with massive MIMO. The developed testbed is capable of realizing MU-MIMO, Massive MIMO, distributed MIMO or Cloud Radio Access Network, etc. The antenna arrays designed in our lab provide 360° azimuth coverage with 48 antenna ports (192 antenna elements) in a circular array. We demonstrated our Massive MIMO work on this testbed, where we proposed a user pairing algorithm and evaluated the performance of the proposed algorithm by implementing it in the said testbed. Our proposed algorithm can multiplex 36 UEs on the same time-frequency resources utilizing 48 antenna ports (192 antenna elements) at BS. In our experiment, 24 UEs out of 36 UEs are paired with the QPSK modulation scheme for a correlation threshold of 0.3 on the same time-frequency resources. To support higher modulation schemes in such a dense environment, 9 and 6 UEs are paired with 16QAM and 64QAM modulation schemes, respectively. With the support of a large number of UEs on the same time-frequency resources, this testbed demonstrates improvement in spectral efficiency to a large extent, which can meet the demands of 5G and beyond systems.

Note that CSI cannot be estimated per tone due to the pilot overhead, which will be too high to estimate per tone CSI. Therefore, per PRB, precoding is required, but it will result in performance losses leading to inter-user interference in the presence of a frequency-selective channel. Such a performance loss grows as the number of users increases. Hence, experiments of this kind will establish bounds on the achievable performance of Ls Massive MIMO under realistic wireless propagation channel conditions using realistic operational algorithms. Therefore, extensive experimental work is essential to determine the achievable gain of Ls Massive MIMO. Hence, in the future, we plan to study the pairing of a large number of users in the context of the outdoor environment and other cell interference to explore the achievable Massive MIMO gains in practice. Further, we will explore new antenna deployment topologies for indoor applications, such as distributed antennas on the roof of a large room, distributed antennas in a building, and outdoor performance on a tower with rectangular, circular, and cylindrical arrays. This testbed will also help to study the improvements in coverage due to massive arrays and flexibly sweeping beams in 360^0 to handle multiple users in multiple cell sites. We will present more results in the future that will discuss these open problems.

ACKNOWLEDGMENT

The authors would like to thank Abhishek Nalam, N. S. Neagin, S. Sai Laxman, and D. Hemaprasad Reddy with IIT Hyderabad in bringing up the testbed.

REFERENCES

[1] *5G;NR; Physical Channels and Modulation*, document TS 38.211, Version 16.2.0, Jul. 2020.
[2] *5G;NR; Multiplexing and Channel Coding*, document TS 38.212, Version 16.2.0, 3GPP, Jul. 2020.

[3] *5G;NR; Physical Layer Procedures for Control*, document TS 38.213, Version 16.2.0, 3GPP, Jul. 2020.
[4] *5G;NR; Physical Layer Procedures for Data*, document TS 38.214, Version 16.2.0, 3GPP, Jul. 2020.
[5] E. Bjornson, J. Hoydis, and L. Sanguinetti, "Massive MIMO has unlimited capacity," *IEEE Trans. Wireless Commun.*, vol. 17, no. 1, pp. 574–590, Jan. 2018.
[6] E. Björnson, E. G. Larsson, and M. Debbah, "Massive MIMO for maximal spectral efficiency: How many users and pilots should be allocated?" *IEEE Trans. Wireless Commun.*, vol. 15, no. 2, pp. 1293–1308, Feb. 2016.
[7] T. L. Marzetta, *Fundamentals of Massive MIMO*. Cambridge, U.K.: Cambridge Univ. Press, 2016.
[8] T. L. Marzetta, "Massive MIMO: An introduction," *Bell Labs Tech. J.*, vol. 20, pp. 11–22, 2015.
[9] L. Lu, G. Y. Li, A. L. Swindlehurst, A. Ashikhmin, and R. Zhang, "An overview of massive MIMO: Benefits and challenges," *IEEE J. Sel. Topics Signal Process.*, vol. 8, no. 5, pp. 742–758, Oct. 2014.
[10] A. J. Paulraj and T. Kailath, "Increasing capacity in wireless broadcast systems using distributed transmission/directional reception," U.S. Patent 5 345 599, Sep. 6, 1994.
[11] A. J. Paulraj, D. A. Gore, R. U. Nabar, and H. Bolcskei, "An overview of MIMO communications—A key to gigabit wireless," *Proc. IEEE*, vol. 92, no. 2, pp. 198–218, Feb. 2004.
[12] E. Telatar, "Capacity of multi-antenna Gaussian channels," *Eur. Trans. Telecommun.*, vol. 10, no. 6, pp. 585–595, Nov. 1999.
[13] G. J. Foschini, "Layered space-time architecture for wireless communication in a fading environment when using multi-element antennas," *Bell Labs Tech. J.*, vol. 1, no. 2, pp. 41–59, Aut. 1996.
[14] G. J. Foschini and M. J. Gans, "On limits of wireless communications in a fading environment when using multiple antennas," *Wireless Pers. Commun.*, vol. 6, no. 3, pp. 311–335, Mar. 1998.
[15] Q. H. Spencer, C. B. Peel, A. L. Swindlehurst, and M. Haardt, "An introduction to the multi-user MIMO downlink," *IEEE Commun. Mag.*, vol. 42, no. 10, pp. 60–67, Oct. 2004.
[16] T. L. Marzetta, "Noncooperative cellular wireless with unlimited numbers of base station antennas," *IEEE Trans. Wireless Commun.*, vol. 9, no. 11, pp. 3590–3600, Nov. 2010.
[17] E. Aryafar, N. Anand, T. Salonidis, and E. W. Knightly, "Design and experimental evaluation of multi-user beamforming in wireless LANs," in *Proc. 16th Annu. Int. Conf. Mobile Comput. Netw.*, Sep. 2010, pp. 197–208.
[18] A. Wiesel, Y. C. Eldar, and S. Shamai, "Zero-forcing precoding and generalized inverses," *IEEE Trans. Signal Process.*, vol. 56, no. 9, pp. 4409–4418, Sep. 2008.
[19] A. Goldsmith, "On the optimality of multiantenna broadcast scheduling using zero-forcing beamforming," *IEEE J. Sel. Areas Commun.*, vol. 24, no. 3, pp. 528–541, Mar. 2006.
[20] M. A. Albreem, A. H. Al Habbash, A. M. Abu-Hundrouss, and S. S. Ikki, "Overview of precoding techniques for massive MIMO," *IEEE Access*, vol. 9, pp. 60764–60801, 2021.
[21] H. Q. Ngo, E. G. Larsson, and T. L. Marzetta, "Energy and spectral efficiency of very large multiuser MIMO systems," *IEEE Trans. Commun.*, vol. 61, no. 4, pp. 1436–1449, Apr. 2013.
[22] F. Rusek, D. Persson, B. K. Lau, E. G. Larsson, T. L. Marzetta, O. Edfors, and F. Tufvesson, "Scaling up MIMO: Opportunities and challenges with very large arrays," *IEEE Signal Process. Mag.*, vol. 30, no. 1, pp. 40–60, Jan. 2013.
[23] A. Sakhnini, S. De Bast, M. Guenach, A. Bourdoux, H. Sahli, and S. Pollin, "Near-field coherent radar sensing using a massive MIMO communication testbed," *IEEE Trans. Wireless Commun.*, vol. 21, no. 8, pp. 6256–6270, Aug. 2022.
[24] A. Saleem, H. Cui, Y. He, and A. Boag, "Channel propagation characteristics for massive multiple-input/multiple-output systems in a tunnel environment [measurements corner]," *IEEE Antennas Propag. Mag.*, vol. 64, no. 3, pp. 126–142, Jun. 2022.
[25] A. Saleem, Y. Xu, R. A. Khan, I. Rasheed, Z. U. A. Jaffri, and M. A. Layek, "Statistical characteristics of 3D MIMO channel model for vehicle-to-vehicle communications," *Wireless Commun. Mobile Comput.*, vol. 2022, pp. 1–14, Jun. 2022.
[26] S. Malkowsky, J. Vieira, L. Liu, P. Harris, K. Nieman, N. Kundargi, I. C. Wong, F. Tufvesson, V. Owall, and O. Edfors, "The world's first real-time testbed for massive MIMO: Design, implementation, and validation," *IEEE Access*, vol. 5, pp. 9073–9088, 2017.
[27] C. Shepard, H. Yu, N. Anand, E. Li, T. Marzetta, R. Yang, and L. Zhong, "Argos: Practical many-antenna base stations," in *Proc. 18th Annu. Int. Conf. Mobile Comput. Netw.*, Aug. 2012, pp. 53–64.
[28] G. Xu, Y. Li, J. Yuan, R. Monroe, S. Rajagopal, S. Ramakrishna, Y. H. Nam, J.-Y. Seol, J. Kim, M. M. U. Gul, A. Aziz, and J. Zhang, "Full dimension MIMO (FD-MIMO): Demonstrating commercial feasibility," *IEEE J. Sel. Areas Commun.*, vol. 35, no. 8, pp. 1876–1886, Aug. 2017.
[29] J. Jeon, G. Lee, A. A. I. Ibrahim, J. Yuan, G. Xu, J. Cho, E. Onggosanusi, Y. Kim, J. Lee, and J. C. Zhang, "MIMO evolution toward 6G: Modular massive MIMO in low-frequency bands," *IEEE Commun. Mag.*, vol. 59, no. 11, pp. 52–58, Nov. 2021.
[30] T. Wirth, T. Haustein, A. Forck, H. Gäbler, K. Krüger, U. Krüger, O. Braz, and C. Schieblich, "Modular concepts for practical massive MIMO implementations," in *Proc. IEEE Radio Wireless Symp. (RWS)*, Jan. 2020, pp. 60–67.
[31] A. Colpaert, S. De Bast, R. Beerten, A. P. Guevara, Z. Cui, and S. Pollin, "Massive MIMO channel measurement data set for localization and communication," *IEEE Commun. Mag.*, vol. 61, no. 9, pp. 114–120, Sep. 2023.
[32] S. Bisoyi, M. M. Pasupuleti, K. Kuchi, K. Rao, H. Kumar, M. P. Reddy, S. Kumari, and S. D. Amuru, "Meeting IMT 2030 performance targets: The potential of OTFDM waveform and structural MIMO technologies," 2023, *arXiv:2307.14978*.
[33] *LTE; Evolved Universal Terrestrial Radio Access (E-UTRA), Physical Channels and Modulation*, document TS 36.211, Version 16.2.0, 3GPP, 2020.
[34] C. A. Balanis, *Antenna Theory: Analysis and Design*. Hoboken, NJ, USA: Wiley, 2005.
[35] *5G;NR; User Equipment (UE) Conformance Specification; Radio Transmission and Reception—Part 1: Range 1 Standalone*, document TS 38.521-1, Version 15.1.0, 3GPP, Apr. 2019.
[36] R. Schmogrow, B. Nebendahl, M. Winter, A. Josten, D. Hillerkuss, S. Koenig, J. Meyer, M. Dreschmann, M. Huebner, C. Koos, J. Becker, W. Freude, and J. Leuthold, "Error vector magnitude as a performance measure for advanced modulation formats," *IEEE Photon. Technol. Lett.*, vol. 24, no. 1, pp. 61–63, Oct. 17, 2011.
[37] H. A. Mahmoud and H. Arslan, "Error vector magnitude to SNR conversion for nondata-aided receivers," *IEEE Trans. Wireless Commun.*, vol. 8, no. 5, pp. 2694–2704, May 2009.

SPANDAN BISOYI received the M.Tech. degree in electrical engineering from IIT Hyderabad, Hyderabad, India, in 2019, where he is currently pursuing the Ph.D. degree. He is also working on the massive MIMO testbed under the guidance of Prof. Kiran Kuchi. He has demonstrated the extreme massive MIMO testbed for sixth-generation systems with India Mobile Congress 2022, Delhi, India. His research interests include massive MIMO and cell-free MIMO technologies for fifth-generation and sixth-generation systems.

PASUPULETI MURALIMOHAN received the M.Tech. degree in electrical engineering from IIT Madras, Chennai, India, in 1990. He is currently pursuing the Ph.D. degree in electrical engineering with IIT Hyderabad, Hyderabad, India. Since 1991, he has been working with DoT on microwave and satellite communication systems in India. Since 2004, he has been in deputation with BSNL. He designed the antenna systems for the massive MIMO with IIT Hyderabad. His research interest includes antenna design for massive MIMO testbed. In 1999, he received the Best Telecom District Award.

HARISH KUMAR DUREPPAGARI received the M.Tech. degree in electrical engineering from IIT Hyderabad, Hyderabad, India, in 2016. He is currently pursuing the Ph.D. degree with the Department of Electrical and Computer Engineering, Virginia Tech, Bradley, USA. From 2017 to 2021, he was with WiSig Networks under the guidance of Prof. Kiran Kuchi. He works on UAV-aided indoor localization for emergency applications jointly advised by Prof. Harpreet S. Dhillon and Prof. R. Michael Bueher with Virginia Tech. His research interests include signal processing for communications and localization, cellular communications, and massive MIMO.

PAVAN REDDY MANNE received the M.Tech. and Ph.D. degrees in electrical engineering from IIT Hyderabad, Hyderabad, India, in 2018 and 2021, respectively. His research interests include physical-layer algorithms and the development of prototypes for fifth-generation systems. He was a recipient of the Excellence in Research Award at IIT Hyderabad, in 2018.

SAIDHIRAJ AMURU received the B.Tech. degree in electrical engineering from IIT Madras, Chennai, India, in 2009, and the Ph.D. degree in electrical and computer engineering from Virginia Tech, in 2015. His Ph.D. advisor with Virginia Tech under the guidance of Dr. R. M. Buehrer. From 2009 to 2011, he was with Qualcomm, India, as a Modem Engineer. From 2014 to 2017, he was a Chief Engineer with the Samsung Research and Development Institute, Bengaluru. Currently, he is the Head of Research and Development with WiSig Networks. Also, he is an Adjunct Assistant Professor with the Department of Electrical Engineering, IIT Hyderabad, Hyderabad, India. His research interests include cognitive radio, statistical signal processing, and online learning. He was a recipient of the Exemplary Reviewer Award of the 2019 IEEE Wireless Communications Letters journal and the Best Paper Award (Honorable Mention) at COMSNETS 2020.

KIRAN KUCHI (Senior Member, IEEE) received the B.Tech. degree in electronics and communications engineering from the Sri Venkateswara University College of Engineering, Tirupati, India, in 1995, and the M.S. and Ph.D. degrees in electrical engineering from The University of Texas at Arlington, Arlington, TX, USA, in 1997 and 2006, respectively. From 2000 to 2008, he was with Nokia Research, Irving, TX, USA, where he contributed to the development of a global system for mobile communication/EDGE, WiMax, and long-term evolution systems. From 2008 to 2011, he was with the Centre of Excellence in Wireless Technology, where he led fourth-generation research and standardization efforts. He was also an Adjunct Faculty with the Department of Electrical Engineering, IIT Madras, Chennai, India. He is currently a Professor with the Department of Electrical Engineering, IIT Hyderabad, Hyderabad, India. He holds more than 20 U.S. patents. His current research interests include physical-layer algorithms and the development of prototypes for fifth-generation and sixth-generation systems.